Spin-1/2 Triangular-Lattice Heisenberg Antiferromagnet with $\sqrt{3} \times \sqrt{3}$-Type Distortion --Behavior around the Boundaries of the Intermediate Phase

AUTHOR(S):

Shimada, Alisa; Nakano, Hiroki; Sakai, Tôru; Yoshimura, Kazuyoshi

J. Phys. Soc. Jpn.
Journal of the Physical Society of Japan **87**, 034706 (2018)
https://doi.org/10.7566/JPSJ.87.034706

Spin-1/2 Triangular-Lattice Heisenberg Antiferromagnet with $\sqrt{3}\times\sqrt{3}$-Type Distortion —Behavior around the Boundaries of the Intermediate Phase

Alisa Shimada[1*], Hiroki Nakano[2†], Tôru Sakai[2,3‡], and Kazuyoshi Yoshimura[1§]

[1]*Graduate School of Science, Kyoto University, Kyoto 606-8502, Japan*
[2]*Graduate School of Material Science, University of Hyogo, Kamigori, Hyogo 678-1297, Japan*
[3]*National Institutes for Quantum and Radiological Science and Technology (QST), SPring-8, Sayo, Hyogo 679-5148, Japan*

(Received November 10, 2017; accepted December 26, 2017; published online February 15, 2018)

The $S = 1/2$ triangular-lattice Heisenberg antiferromagnet with distortion is investigated by the numerical-diagonalization method. The examined distortion type is $\sqrt{3}\times\sqrt{3}$. We study the case when the distortion connects the undistorted triangular lattice and the dice lattice. For the intermediate phase reported previously in this system, we obtain results of the boundaries of the intermediate phase for a larger system than those in the previous report and examine the system size dependence of the boundaries in detail. We also report the specific heat of this system, which shows a marked peak structure related to the appearance of the intermediate state.

1. Introduction

Frustration has been attracting increasing attention because it often becomes a source of nontrivial phenomena in various physical systems. Among them, frustrated magnets are extensively studied from various viewpoints. The triangular-lattice antiferromagnet is a typical example of such frustrated systems. Particularly, Anderson's suggestion[1] that the $S = 1/2$ triangular-lattice Heisenberg antiferromagnet is a possible candidate for the realization of a spin-liquid ground state owing to frustrations accelerated investigations of this system from not only theoretical approaches[2–15] but also experimental ones.[16,17] Although the kagome-lattice antiferromagnet is another typical example,[18–38] it is widely considered that the understanding of the triangular-lattice antiferromagnet is deeper than that of the kagome-lattice antiferromagnet. Many researchers believe that the symmetry-breaking state with the so-called 120-degree structure is realized in the ground state of the $S = 1/2$ triangular-lattice Heisenberg antiferromagnet. However, a recent study based on a large-scale numerical calculation has suggested the absence of such symmetry breaking;[39] the issue concerning the ground state is still controversial up to now.

When the triangular-lattice antiferromagnet is experimentally realized, effects due to distortions in the perfect structure of the triangular lattice should be examined. The reason for this is that some distortions often occur in the experimentally planned structure. A one-dimensional distortion in the triangular lattice has been investigated.[40–42] Since distortions are not necessarily uniform, random distortions in interaction bonds are also studied.[43,44] Even within cases of a uniform distortion, however, the types of distortion are not limited to the one-dimensional distortion.

A recent study has shown that there is an intermediate phase of spontaneously magnetized states with its magnitude varying continuously in the triangular-lattice antiferromagnet with the $\sqrt{3}\times\sqrt{3}$-type distortion.[45] The distortion links two cases: one is the triangular lattice and the other is the dice lattice. In the former case, the ground state does not show a spontaneous magnetization regardless of whether the ground state reveals symmetry breaking. In the latter case, on the other hand, the ground state of the dice-lattice antiferromagnet is the so-called up–up–down (UUD) state showing the spontaneous magnetization with its magnitude being one third of the saturation magnetization. The UUD state is a ferrimagnetic state, which can be explained by the Marshall–Lieb–Mattis theorem.[46,47] The phase of intermediate states appears between the phase of the vanishing spontaneous magnetization and the phase of the spontaneous magnetization, which is one third of the saturation magnetization.

The purpose of this study is to present novel information on the transitions at the boundary between the vanishing spontaneous magnetization phase and the intermediate phase and at the boundary between the intermediate phase and the UUD ferrimagnetic phase from two aspects. One is the position of the boundaries at zero temperature. We additionally present the results of a system larger than those treated in Ref. 45. The results confirm the existence of the intermediate phase with a nonzero width. The other is the temperature dependence of the specific heat of this system. From the behavior of the specific heat, one can find the relationship between the structure in the specific heat and the appearance of the phase transitions. As a study concerning the temperature dependences of physical quantities, Bonner and Fisher's work[48] is widely known, in which the one-dimensional chain model of the $S = 1/2$ Heisenberg antiferromagnet was investigated by numerical diagonalizations. Although other different numerical algorithms have been developed after Ref. 48, available methods are still limited for frustrated systems in spatial dimensions larger than one. Under this situation, our understanding of the temperature dependences of physical quantities of two-dimensional frustrated systems is insufficient even now. In this paper, we report such results for the triangular-lattice antiferromagnet with the $\sqrt{3}\times\sqrt{3}$-type distortion.

This paper is organized as follows. In the next section, the model that we study here is introduced. The method is also explained. The third section is devoted to the presentation and discussion of our results. We first report the system size dependence of the boundaries including results for a larger size. Next, we present the results of the specific heat. The characteristic peak structure is discussed. In the final section, we present the conclusion drawn from this study.

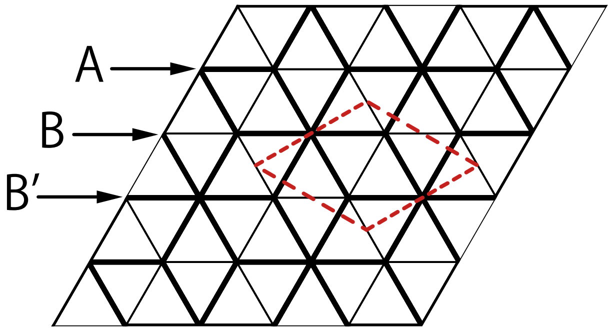

Fig. 1. (Color online) Triangular lattice with a distortion of the $\sqrt{3}\times\sqrt{3}$ type. The thin and thick solid lines denote the bonds of interaction, J_1 and J_2, respectively. Its unit cell is illustrated by the red broken line. The vertices of the lattice are divided into three sublattices A, B, and B′.

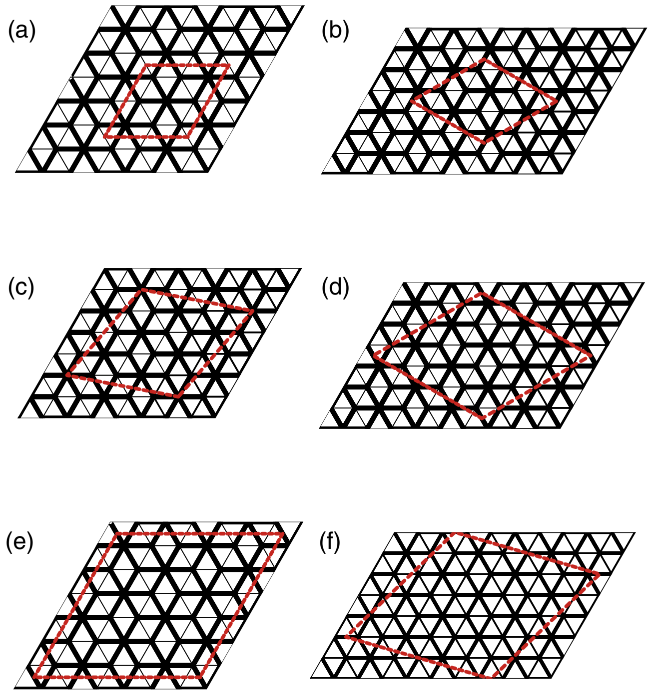

Fig. 2. (Color online) Shapes of finite-size clusters. The rhombuses of red broken lines in Panels (a)–(f) denote the clusters for N_s = 9, 12, 21, 27, 36, and 39, respectively.

2. Model Hamiltonian and Method

The Hamiltonian studied in this paper is given by

$$\mathcal{H} = \sum_{i\in\mathrm{B},j\in\mathrm{B}'} J_1 \boldsymbol{S}_i\cdot\boldsymbol{S}_j + \sum_{i\in\mathrm{A},j\in\mathrm{B}} J_2 \boldsymbol{S}_i\cdot\boldsymbol{S}_j + \sum_{i\in\mathrm{A},j\in\mathrm{B}'} J_2 \boldsymbol{S}_i\cdot\boldsymbol{S}_j. \tag{1}$$

Here, $\boldsymbol{S}_i$ denotes the $S=1/2$ spin operator at site i. In this paper, we consider the case of isotropic interaction in spin space. Site i is assumed to be the vertices of the triangular lattice, which is illustrated in Fig. 1. The number of spin sites is represented by N_s. The vertices are divided into three sublattices A, B, and B′. Each site i in the A sublattice is connected by six interaction bonds J_2 represented by thick lines. Each site i in the B or B′ sublattice is connected by three interaction bonds J_2 and three interaction bonds J_1, represented by thin lines. The ratio of J_2/J_1 is denoted by r. All interactions are considered to be antiferromagnetic, namely, $J_1>0$ and $J_2>0$. Energies are measured in J_1 units. We hereafter set $J_1=1$. Here, we examine the case of $J_2\geq J_1$. Note that, for $J_1=J_2$, namely, $r=1$, the present lattice is identical to the triangular lattice. It is well known that the ground state of the triangular-lattice antiferromagnet does not reveal nonzero spontaneous magnetizations. On the other hand, for $J_1\to 0$, namely, $r\to\infty$, the network of the vertices becomes the dice lattice.

The finite-size clusters treated in this study are depicted in Fig. 2. We examine the cases of N_s = 9, 12, 21, 27, 36, and 39 under the periodic boundary condition. Note here that the case of $N_\mathrm{s}=39$ is additionally tackled in the present paper. In all the cases, $N_\mathrm{s}/3$ is an integer; therefore, the number of spin sites in a sublattice is the same regardless of sublattices. The clusters are rhombic and have an inner angle $\pi/3$; this shape allows us to capture two dimensionality well.

We use two algorithms among numerical-diagonalization methods. The numerical-diagonalization calculations are unbiased against any approximations. One can therefore obtain reliable information on the system. By the method based on the Lanczos algorithm, we calculate the lowest energy of $\mathcal{H}$ in the subspace characterized by $\sum_j S_j^z = M$. The lowest energy within the subspace for M is denoted by $E_0(N_\mathrm{s}, M)$, where M takes an integer or a half odd integer up to the saturation value M_sat $(=N_\mathrm{s}/2)$. We define M_spo as the largest M among the lowest-energy states, because M_spo corresponds to the spontaneous magnetization at zero temperature. Note, first, that in cases of odd N_s, the smallest M_spo cannot vanish; the result of $M_\mathrm{spo}=1/2$ in the ground state indicates that the system does not reveal spontaneous magnetization. We also use the normalized magnetization $m=M_\mathrm{spo}/M_\mathrm{sat}$. Some of the Lanczos diagonalizations were carried out using an MPI-parallelized code, which was originally developed in the study of Haldane gaps.[49] The usefulness of our program was confirmed in large-scale parallelized calculations.[42,50–52] On the other hand, by the method based on the Householder algorithm, we calculate all the energy levels of $\mathcal{H}$, which are denoted by $E_i(N_\mathrm{s}, M)$, where i is the label of energy levels in the subspace of M for the N_s-site system. From the obtained $E_i(N_\mathrm{s}, M)$, one can evaluate the thermal average of the energy at nonzero temperature.

3. Results and Discussion

3.1 *Boundaries of the intermediate phase*

First, let us explain how to determine phase boundaries, which will be defined later, for each N_s from numerical-diagonalization data. Before determining r_c1 and r_c2, we have to find M_spo for given N_s and r. Figure 3 depicts the M-dependence of the lowest-energy levels for given N_s and M. For $r=1$ in the case of $N_\mathrm{s}=36$, no degeneracy appears, which indicates that the spontaneous magnetization vanishes. For $r=1$ in the case of $N_\mathrm{s}=27$, on the other hand, the levels for $M=\pm1/2$ are degenerate, namely, $M_\mathrm{spo}=1/2$; however, $M=\pm1/2$ for odd N_s also means that the spontaneous magnetization vanishes. The situations for $r=1.5$ and 2 are different from that for $r=1$. Nontrivial degeneracy clearly appears regardless of whether N_s is even or odd. Such degeneracy gives M_spo for each N_s and r (see arrows in Fig. 3).

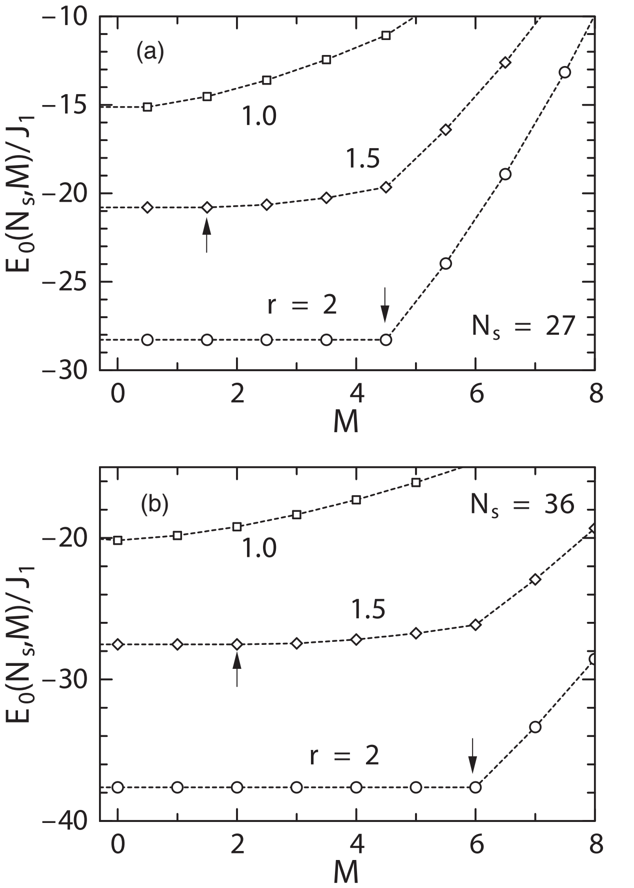

Fig. 3. M dependence of the lowest-energy levels for $N_s = 27$ and 36 in panels (a) and (b), respectively. The results for $r = 1$, 1.5, and 2 are denoted by squares, diamonds, and circles, respectively. The arrows indicate the maximum of M among degenerate ground states in each case of $r = 1.5$ and 2. For $r = 1$, the energy for the smallest $|M|$, namely, $M = 1/2$ for $N_s = 27$ and $M = 0$ for $N_s = 36$, is lower than those for larger $|M|$ for each N_s.

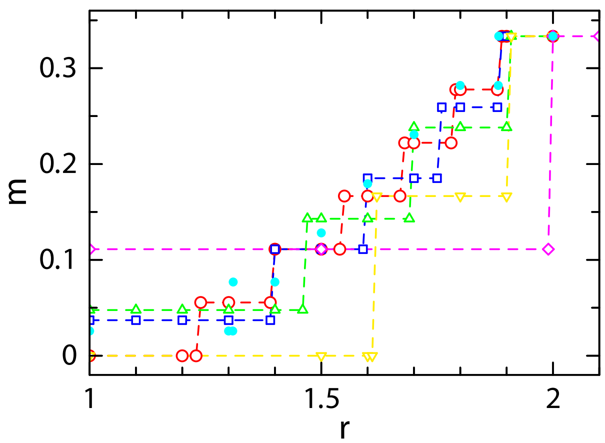

Fig. 4. (Color online) r dependences of the spontaneous magnetization for various system sizes. The violet diamonds, yellow reversed triangles, green triangles, dark blue squares, red circles, and light blue closed circles denote results for $N_s = 9$, 12, 21, 27, 36, and 39, respectively.

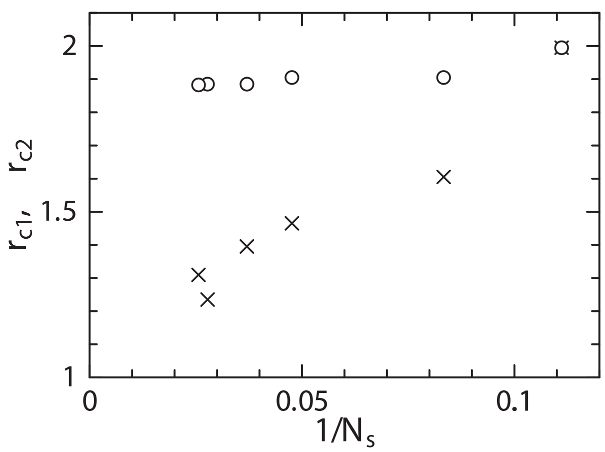

Fig. 5. Size dependences of the phase boundaries r_{c1} and r_{c2}. The crosses and circles denote the results for r_{c1} and r_{c2}, respectively.

Next, let us observe the r dependence of m $(= M_{spo}/M_{sat})$ obtained from the above analysis of $E_0(N_s, M)$. Results for various N_s values are depicted in Fig. 4. Numerical data up to $N_s = 36$ were reported in Ref. 45; data for $N_s = 39$ are additionally presented. Not only for N_s up to 36 but also for $N_s = 39$ are the states of all possible M_{spo} realized between the smallest M_{spo} and $(1/3)M_{sat}$. From the r dependence of m for a given N_s, one finds r_{c1} and r_{c2}. The boundary r_{c1} is defined at r where M_{spo} increases from the smallest M_{spo}, namely, $M_{spo} = 0$ for an even N_s and $M_{spo} = 1/2$ for an odd N_s, to a larger M_{spo}. One also finds r_{c2} where M_{spo} increases to $(1/3)M_{sat}$ from the smaller M_{spo}.

Next, let us, examine the system size dependences of r_{c1} and r_{c2}. Figure 5 depicts our numerical results for the dependence; data for $N_s = 39$ are added from Ref. 45. Results for r_{c2} show a very small size dependence, which strongly suggests $r_{c2} \sim 1.9$ as the extrapolated value to the thermodynamic limit. On the other hand, the dependence of r_{c1} is not so simple. Up to $N_s = 36$, r_{c1} decreases; however, r_{c1} for $N_s = 39$ is larger than r_{c1} for $N_s = 36$. Note that r_{c1} determinations are slightly different between even and odd N_s values. For an even N_s, r_{c1} is obtained at the point from $M_{spo} = 0$ to $M_{spo} = 1$; for an odd N_s, on the other hand, r_{c1} is obtained at the point from $M_{spo} = 1/2$ to $M_{spo} = 3/2$. If one sees four data points for an odd N_s, namely, $N_s = 9$, 21, 27, and 39, the N_s^{-1} dependence of r_{c1} seems quite linear. This linear dependence suggests $r_{c1} \sim 1.1$ as the extrapolated value to the thermodynamic limit. On the other hand, it is unclear whether the results for an even N_s show a linear dependence because there are only two data points. Even if we assume the linear dependence for the two data points, the extrapolated value is not much different from $r_{c1} \sim 1.1$ obtained from odd N_s. This small difference does not contradict the expectation that the values extrapolated from the two series of even and odd N_s values are supposed to converge to a unique value. Therefore, the present analysis suggests that there are two phase boundaries, r_{c1} and r_{c2}, and that the intermediate phase certainly exists in the thermodynamic limit.

The decrease in r from infinity corresponds to an examination concerning a destabilization of the UUD ferrimagnetic state on the side of the dice lattice. It is well known that the UUD state also appears in the Heisenberg antiferromagnet on the so-called Lieb lattice. Destabilizations of the UUD state in the Lieb-lattice antiferromagnet were studied in various systems.[53–59] However, there are both the presence and absence of intermediate states with nontrivial spontaneous magnetizations. The origin of this difference between the presence and absence is unclear at present. The question of what is the origin should be clarified. The examination of the UUD state in the dice-lattice case has just been started; studying the behaviors of the systems with various types of competing interactions is a future issue.

In the present study, we examine the case of $r \geq 1$. It is considered that the $\sqrt{3}\times\sqrt{3}$-type distortion in the triangular-lattice antiferromagnet is experimentally realized.[60,61] However, Refs. 60 and 61 showed that the ratios corresponding to these materials are smaller than unity. The ratios are outside of the region studied in the present work. The behavior of a system in the region of $r \leq 1$ was investigated theoretically,[62] which clarified the appearance of other states with nonzero spontaneous magnetization. Reference 62 showed that when r is decreased from $r = 1$, the spontaneous magnetization grows gradually from $M_{\rm spo} = 1$ to $M_{\rm spo} = (1/3)M_{\rm sat} - 1$; states of possible $M_{\rm spo}$ are certainly realized. The growth for $r \leq 1$ is common with that for $r \geq 1$. However, the spontaneous magnetization does not reach $M_{\rm spo} = (1/3)M_{\rm sat}$; instead, the spontaneous magnetization disappears suddenly. The disappearance for $r \leq 1$ is different from the behavior for $r \geq 1$; the reason for the disappearance is still unresolved. The relationship between the experimental observation and the theoretical finding should be examined in the future.

3.2 *Specific heat*

We examine the specific heat of the system. We evaluate it as

$$C = \frac{\partial \langle E \rangle}{\partial T}. \tag{2}$$

Here, T is the temperature and $\langle E \rangle$ is the thermal average of the energy obtained by

$$\langle E \rangle = \frac{\sum_{i,M} E_i(N_{\rm s}, M)\exp[-E_i(N_{\rm s}, M)/(kT)]}{\sum_{i,M} \exp(-E_i(N_{\rm s}, M)/(kT))}, \tag{3}$$

where k is the Boltzmann constant. Here, we calculate the specific heat of the system only for $N_{\rm s} = 12$ because available computer resources are insufficient for a larger $N_{\rm s}$. Recall that, in Fig. 5, the boundaries for $N_{\rm s} = 12$ are $r_{\rm c1} \sim 1.612$ and $r_{\rm c2} \sim 1.906$.

Now, let us observe the temperature dependence of the specific heat. Figure 6 depicts the results of the specific heat for $r = 1$–1.6. For $r = 1$ corresponding to the undistorted triangular-lattice antiferromagnet, the specific heat shows a large peak at $kT/J_1 \sim 0.28$ together with a faint shoulder at $kT/J_1 \sim 0.9$. Particularly, the large peak is a characteristic behavior of the undistorted triangular-lattice antiferromagnet. The behavior of the peak and shoulder has already been observed in Ref. 63, which presented the result obtained using the finite-temperature Lanzcos method. When the $\sqrt{3}\times\sqrt{3}$-type distortion is switched on, this characteristic peak becomes smaller, and the shoulder for $r = 1$ around $kT/J_1 \sim 0.9$ becomes a broad peak. For $r \sim 1.4$, the broad peak becomes larger than the peak around $kT/J_1 \sim 0.3$. Furthermore, another shoulder appears around $kT/J_1 \sim 0.1$. For a larger r, the broad peak gradually moves to a higher temperature. On the other hand, one finds that the new shoulder for $r \sim 1.4$ becomes a small but significant peak for $r \sim 1.5$, which is rather close to $r_{\rm c1}$ for $N_{\rm s} = 12$.

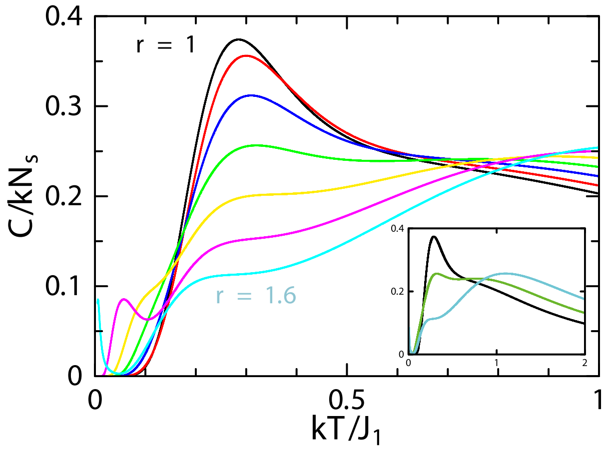

Fig. 6. (Color online) Temperature dependences of the specific heat for $N_{\rm s} = 12$ of the $S = 1/2$ Heisenberg antiferromagnet on the triangular lattice with the $\sqrt{3}\times\sqrt{3}$-type distortion. The specific heat is given for $r = 1$, 1.1, 1.2, 1.3, 1.4, 1.5, and 1.6 by the black, red, dark blue, green, yellow, violet, and light blue lines, respectively. The inset depicts the same curves for $r = 1$, 1.3, and 1.6 by the same colors in a wide temperature range.

To clarify the relationship between the low-temperature peak behavior and the zero-temperature phase transition at $r = r_{\rm c1}$, let us observe the specific heat in a low-temperature region in detail; Fig. 7(a) depicts the results for $r = 1.40$, 1.45, 1.50, 1.55, and 1.60. One can observe that the low-temperature peak moves from high temperature to low temperature as r is increased. For $r = 1.60$, the low-temperature peak and the higher-temperature broad structure become markedly separated from each other. The marked separation enables us to examine the weight of the low-temperature peak from the viewpoint of the entropy given by $S(T) = \int_0^T (C/T)dT$. Note here that the entropy of this system is supposed to satisfy $\lim_{T\to\infty}[S(T)/N_{\rm s}k] = \ln 2$. Our numerical results show $S(T = 0.05J_1/k)/\ln 2 \sim 0.17$. This quantity suggests that the low-temperature peak has a significant weight coming from a macroscopic number of states. In Fig. 7(b) in which results for $r = 1.625$, 1.630, 1.635, 1.640, and 1.645 are presented, on the other hand, the low-temperature peak moves from a low temperature to a high temperature as r is increased. To capture the behavior of this low-temperature peak in more detail, the r dependence of the temperature of the peak denoted by $T_{\rm peak}$ is examined; results are depicted in Fig. 8. The peak temperature in the region of r smaller than $r_{\rm c1}$ certainly approaches $r_{\rm c1}$ at zero temperature. The peak temperature in the region of r larger than $r_{\rm c1}$ also approaches $r_{\rm c1}$ at zero temperature. This strongly suggests that the behavior of the peak is related to the phase transition at $r = r_{\rm c1}$ at zero temperature. This means that the intermediate state between $r_{\rm c1}$ and $r_{\rm c2}$ has its origin in the peak characterizing the undistorted triangular-lattice antiferromagnet. The seed of the intermediate state is part of the states producing the peak around $kT/J_1 \sim 0.28$ for $r = 1$. As the distortion becomes larger, the seed separates from other states. With further increase in distortion, the seed forms a low-temperature peak that approaches zero temperature. When the peak meets zero temperature, the phase transition finally occurs and the intermediate state appears between $r_{\rm c1}$ and $r_{\rm c2}$ as the ground state of the system. If these observed behaviors are assumed to survive in the thermody-

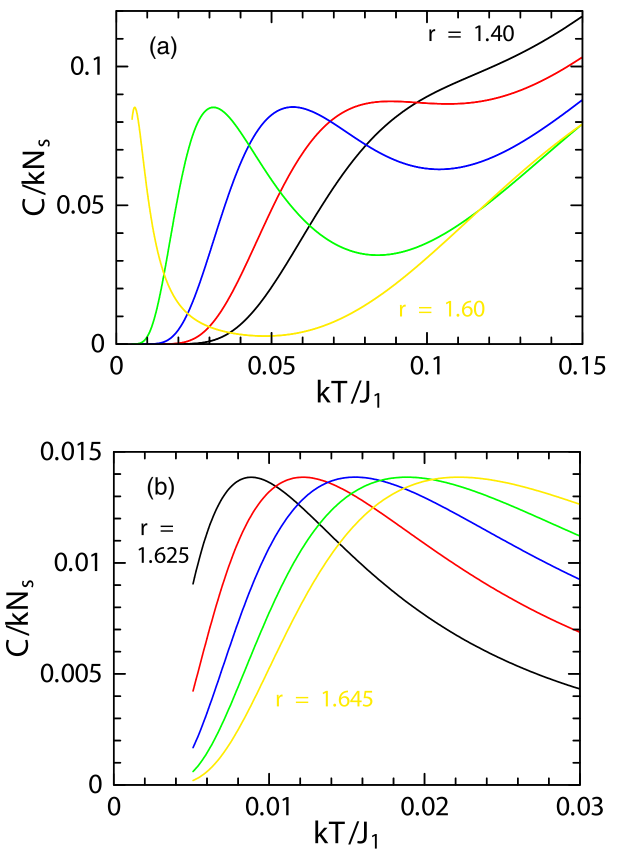

Fig. 7. (Color online) Zoom-in views around $r = r_{c1}$ for temperature dependences of the specific heat for $N_s = 12$ of the $S = 1/2$ Heisenberg antiferromagnet on the triangular lattice with the $\sqrt{3} \times \sqrt{3}$-type distortion. Panel (a) depicts the side of r smaller than r_{c1}. The specific heat is given for $r = 1.40$, 1.45, 1.50, 1.55, and 1.60 by the black, red, dark blue, green, and yellow lines, respectively. Panel (b) depicts the side of r larger than r_{c1}. The specific heat is given for $r = 1.625$, 1.630, 1.635, 1.640, and 1.645 by the black, red, dark blue, green, and yellow lines, respectively.

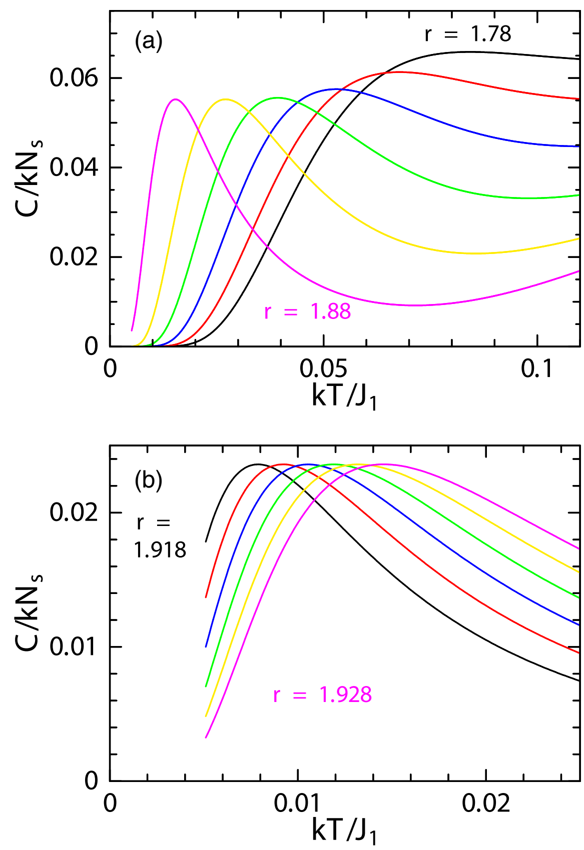

Fig. 9. (Color online) Zoom-in views around $r = r_{c2}$ for temperature dependences of the specific heat for $N_s = 12$ of the $S = 1/2$ Heisenberg antiferromagnet on the triangular lattice with the $\sqrt{3} \times \sqrt{3}$-type distortion. Panel (a) depicts the side of r smaller than r_{c2}. The specific heat is given for $r = 1.78$, 1.80, 1.82, 1.84, 1.86, and 1.88 by the black, red, dark blue, green, yellow, and violet lines, respectively. Panel (b) depicts the side of r larger than r_{c2}. The specific heat is given for $r = 1.918$, 1.920, 1.922, 1.924, 1.926, and 1.928 by the black, red, dark blue, green, yellow, and violet lines, respectively.

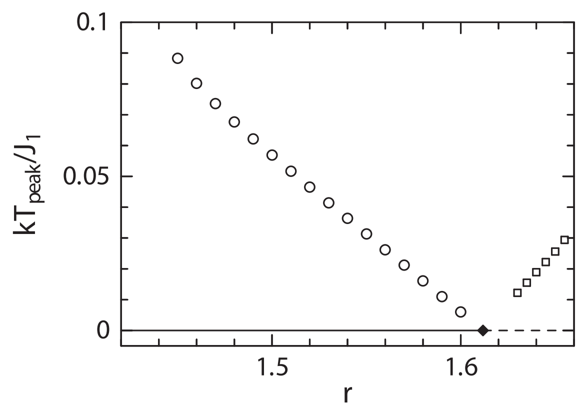

Fig. 8. r dependence of the temperature of the small peak around $r = r_{c1}$ in the $N_s = 12$ specific heat of the $S = 1/2$ Heisenberg antiferromagnet on the triangular lattice with the $\sqrt{3} \times \sqrt{3}$-type distortion. The open circles (squares) denote results for r smaller (larger) than r_{c1}. The horizontal lines at zero temperature represent the ground-state behavior. The solid and broken lines indicate the vanishing spontaneous magnetization phase and intermediate phase, respectively. The closed diamond denotes $r = r_{c1}$ for $N_s = 12$.

namic limit, the system around $r = r_{c1}$ shows that a macroscopic number of excited states degenerate with the ground state; the degeneracy produces a significant residual entropy. Our results strongly suggest the relationship between the residual entropy and the occurrence of the phase transition at $r = r_{c1}$.

We are, then, faced with a question of what happens around $r = r_{c2}$. The behavior of the low-temperature peak is presented in Figs. 9(a) and 9(b) in the region of r smaller and larger than r_{c2}, respectively. The low-temperature peak also appears around $r = r_{c2}$. The movement of this peak around $r = r_{c2}$ is similar to that around $r = r_{c1}$. The change in the temperature of the peak is clearly depicted in Fig. 10. One finds that the temperature of the peak approaches r_{c2} at zero temperature. This behavior also suggests that the behavior of the low-temperature peak is related to the phase transition at $r = r_{c2}$ at zero temperature.

In the present paper, we cannot calculate the specific heat for N_s larger than $N_s = 12$. Therefore, the system size dependence of the peak behavior is not examined at present. Specific values such as $r_{c1} \sim 1.612$ and $r_{c2} \sim 1.906$ are just for $N_s = 12$. Further investigation of the specific heat for a larger N_s should be carried out in the future. A method applicable to the present system is the Hams–de Raedt algorithm,[64] which was applied to the resolution of the issue of the specific heat of the $N_s = 36$ kagome-lattice antiferromagnet.[38] Results for larger systems could make us capture the behavior of this system more quantitatively including the system size dependence. The investigation

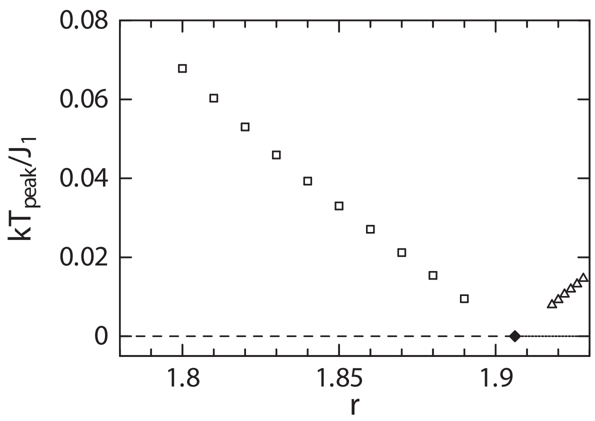

Fig. 10. r dependence of the temperature of the small peak around $r = r_{c2}$ in the $N_s = 12$ specific heat of the $S = 1/2$ Heisenberg antiferromagnet on the triangular lattice with the $\sqrt{3} \times \sqrt{3}$-type distortion. The open squares (triangles) denote results for r smaller (larger) than r_{c2}. The horizontal lines at zero temperature represent the ground-state behavior. The broken and solid lines indicate the intermediate phase and UUD-ferrimagnetic phase, respectively. The closed diamond denotes $r = r_{c2}$ for $N_s = 12$.

would deepen our understanding concerning the behavior of the specific heat.

A similar multipeak behavior in the temperature dependence of the specific heat was reported in other systems.[65–67] From this similarity, these systems may possibly become a clue for a deeper understanding of the present system. In these systems, the behavior appears regardless of whether the interaction is of the Heisenberg type or of the Ising type. On the other hand, the common lattice structure in these systems is the diamond shape in each system. The diamond shape is the origin of the fact that the ground state is rigorously obtained. Beyond such a highly ideal situation, the present case suggests that there exists a multipeak behavior in a more realistic system and that a significant change is provided by varying a distortion. In addition, a considerable difference between these diamond systems and the present system is whether the spontaneous magnetization in the ground state is absent or present. Further comparison should be examined in the future.

4. Conclusions

We have investigated the spin-1/2 Heisenberg antiferromagnet on the triangular lattice with $\sqrt{3} \times \sqrt{3}$-type distortion by the numerical-diagonalization method. We have obtained results for a system larger than those in a previous study and examined the system size dependences of the boundaries r_{c1} and r_{c2} of the intermediate-state phase. The existence of the intermediate phase becomes evident. We have also studied the temperature dependence of the specific heat and found the appearance of a new low-temperature peak, which is related to the transition at r_{c1}. An important finding is that the origin of the intermediate state exists as an excited state of the undistorted triangular-lattice antiferromagnet and that the intermediate state plays a role as part of the elements forming the peak for $r = 1$. Our findings concerning the present system are a kind of distortion effect in a two-dimensional frustrated system. Such examinations of other frustrated systems with various distortions would contribute much to our understanding of the frustration effect in quantum spin systems.

Acknowledgments We wish to thank Professor N. Todoroki for fruitful discussions. This work was partly supported by JSPS KAKENHI Grant Numbers 16K05418, 16K05419, and 16H01080 (JPhysics). Nonhybrid thread-parallel calculations in numerical diagonalizations were based on TITPACK version 2 coded by H. Nishimori. This research used computational resources of the K computer provided by the RIKEN Advanced Institute for Computational Science and Oakforest-PACS provided by JCAHPC through the HPCI System Research projects (Project ID: hp170017, hp170028, hp170070, and hp170207). Some of the computations were performed using the facilities of the Department of Simulation Science, National Institute for Fusion Science; Institute for Solid State Physics, The University of Tokyo; and Supercomputing Division, Information Technology Center, The University of Tokyo. This work was partly supported by the Strategic Programs for Innovative Research; the Ministry of Education, Culture, Sports, Science and Technology of Japan; and the Computational Materials Science Initiative, Japan.

*a.shimada@kinso.kuchem.kyoto-u.ac.jp
†hnakano@sci.u-hyogo.ac.jp
‡sakai@spring8.or.jp
§kyhv@kuchem.kyoto-u.ac.jp

1) P. W. Anderson, Mater. Res. Bull. **8**, 153 (1973).
2) D. A. Huse and V. Elser, Phys. Rev. Lett. **60**, 2531 (1988).
3) Th. Jolicoeur and J. C. Le Guillou, Phys. Rev. B **40**, 2727(R) (1989).
4) R. R. P. Singh and D. A. Huse, Phys. Rev. Lett. **68**, 1766 (1992).
5) B. Bernu, C. Lhuillier, and L. Pierre, Phys. Rev. Lett. **69**, 2590 (1992).
6) A. V. Chubukov and Th. Jolicoeur, Phys. Rev. B **46**, 11137 (1992).
7) B. Bernu, P. Lecheminant, C. Lhuillier, and L. Pierre, Phys. Rev. B **50**, 10048 (1994).
8) P. W. Leung and K. J. Runge, Phys. Rev. B **47**, 5861 (1993).
9) P. Lecheminant, B. Bernu, C. Lhuillier, and L. Pierre, Phys. Rev. B **52**, 6647 (1995).
10) J. Richter, J. Schulenburg, and A. Honecker, *Lecture Notes in Physics* (Springer, Heidelberg, 2004) Vol. 645, p. 85.
11) J. Alicea, A. V. Chubukov, and O. A. Starykh, Phys. Rev. Lett. **102**, 137201 (2009).
12) T. Sakai and H. Nakano, Phys. Rev. B **83**, 100405(R) (2011).
13) D. Yamamoto, G. Marmorini, and I. Danshita, Phys. Rev. Lett. **112**, 127203 (2014).
14) O. A. Starykh, Rep. Prog. Phys. **78**, 052502 (2015).
15) H. Nakano and T. Sakai, J. Phys. Soc. Jpn. **86**, 114705 (2017).
16) Y. Shirata, H. Tanaka, A. Matsuo, and K. Kindo, Phys. Rev. Lett. **108**, 057205 (2012).
17) Y. Shirata, H. Tanaka, T. Ono, A. Matsuo, K. Kindo, and H. Nakano, J. Phys. Soc. Jpn. **80**, 093702 (2011).
18) S. Sachdev, Phys. Rev. B **45**, 12377 (1992).
19) T. Nakamura and S. Miyashita, Phys. Rev. B **52**, 9174 (1995).
20) P. Lecheminant, B. Bernu, C. Lhuillier, L. Pierre, and P. Sindzingre, Phys. Rev. B **56**, 2521 (1997).
21) Ch. Waldtmann, H.-U. Everts, B. Bernu, C. Lhuillier, P. Sindzingre, P. Lecheminant, and L. Pierre, Eur. Phys. J. B **2**, 501 (1998).
22) F. Mila, Phys. Rev. Lett. **81**, 2356 (1998).
23) K. Hida, J. Phys. Soc. Jpn. **70**, 3673 (2001).
24) M. Hermele, T. Senthil, and M. P. A. Fisher, Phys. Rev. B **72**, 104404 (2005).
25) R. R. P. Singh and D. A. Huse, Phys. Rev. B **76**, 180407(R) (2007).
26) Y. Ran, M. Hermele, P. A. Lee, and X.-G. Wen, Phys. Rev. Lett. **98**, 117205 (2007).
27) H. C. Jiang, Z. Y. Weng, and D. N. Sheng, Phys. Rev. Lett. **101**, 117203 (2008).
28) O. Cépas, C. M. Fong, P. W. Leung, and C. Lhuillier, Phys. Rev. B **78**, 140405(R) (2008).
29) P. Sindzingre and C. Lhuillier, Europhys. Lett. **88**, 27009 (2009).
30) H. Nakano and T. Sakai, J. Phys. Soc. Jpn. **79**, 053707 (2010).
31) G. Evenbly and G. Vidal, Phys. Rev. Lett. **104**, 187203 (2010).
32) S. Capponi, O. Derzhko, A. Honecker, A. M. Läuchli, and J. Richter, Phys. Rev. B **88**, 144416 (2013).
33) Y. Iqbal, D. Poilblanc, and F. Becca, Phys. Rev. B **89**, 020407(R) (2014).
34) Y. Iqbal, D. Poilblanc, and F. Becca, Phys. Rev. B **91**, 020402(R) (2015).
35) S. Yan, D. A. Huse, and S. W. White, Science **332**, 1173 (2011).

36) S. Depenbrock, I. P. McCulloch, and U. Schollwöck, Phys. Rev. Lett. **109**, 067201 (2012).
37) H. Nakano and T. Sakai, J. Phys. Soc. Jpn. **84**, 063705 (2015).
38) T. Shimokawa and H. Kawamura, J. Phys. Soc. Jpn. **85**, 113702 (2016).
39) S. A. Kulagin, N. Prokof'ev, O. A. Starykh, B. Svistunov, and C. N. Varney, Phys. Rev. Lett. **110**, 070601 (2013).
40) O. A. Starykh and L. Balents, Phys. Rev. Lett. **98**, 077205 (2007).
41) K. Harada, Phys. Rev. B **86**, 184421 (2012).
42) H. Nakano, S. Todo, and T. Sakai, J. Phys. Soc. Jpn. **82**, 043715 (2013).
43) K. Watanabe, H. Kawamura, H. Nakano, and T. Sakai, J. Phys. Soc. Jpn. **83**, 034714 (2014).
44) T. Shimokawa, K. Watanabe, and H. Kawamura, Phys. Rev. B **92**, 134407 (2015).
45) H. Nakano and T. Sakai, J. Phys. Soc. Jpn. **86**, 063702 (2017).
46) W. Marshall, Proc. R. Soc. London, Ser. A **232**, 48 (1955).
47) E. Lieb and D. Mattis, J. Math. Phys. (N.Y.) **3**, 749 (1962).
48) J. C. Bonner and M. E. Fisher, Phys. Rev. **135**, A640 (1964).
49) H. Nakano and A. Terai, J. Phys. Soc. Jpn. **78**, 014003 (2009).
50) H. Nakano and T. Sakai, J. Phys. Soc. Jpn. **80**, 053704 (2011).
51) H. Nakano and T. Sakai, J. Phys. Soc. Jpn. **83**, 104710 (2014).
52) H. Nakano, Y. Hasegawa, and T. Sakai, J. Phys. Soc. Jpn. **84**, 114703 (2015).
53) H. Nakano and T. Sakai, Jpn. J. Appl. Phys. **54**, 030305 (2015).
54) H. Nakano, T. Shimokawa, and T. Sakai, J. Phys. Soc. Jpn. **80**, 033709 (2011).
55) T. Shimokawa and H. Nakano, J. Phys. Soc. Jpn. **81**, 084710 (2012).
56) H. Nakano, M. Isoda, and T. Sakai, J. Phys. Soc. Jpn. **83**, 053702 (2014).
57) M. Isoda, H. Nakano, and T. Sakai, J. Phys. Soc. Jpn. **83**, 084710 (2014).
58) H. Nakano and T. Sakai, J. Phys. Soc. Jpn. **82**, 083709 (2013).
59) H. Nakano, T. Sakai, and Y. Hasegawa, J. Phys. Soc. Jpn. **83**, 084709 (2014).
60) H. Tanaka and K. Kakurai, J. Phys. Soc. Jpn. **63**, 3412 (1994).
61) Y. Nishiwaki, A. Osawa, K. Kakurai, K. Kaneko, M. Tokunaga, and T. Kato, J. Phys. Soc. Jpn. **80**, 084711 (2011).
62) A. Shimada, T. Sakai, H. Nakano, and K. Yoshimura, to be published in J. Phys.: Conf. Ser.
63) T. Koretsune, M. Udagawa, and M. Ogawa, Phys. Rev. B **80**, 075408 (2009).
64) A. Hams and H. De Raedt, Phys. Rev. E **62**, 4365 (2000).
65) L. Čanová, J. Strečka, and M. Jaščur, J. Phys.: Condens. Matter **18**, 4967 (2006).
66) H. Kobayashi, Y. Fukumoto, and A. Oguchi, J. Phys. Soc. Jpn. **78**, 074004 (2009).
67) K. Hida, K. Takano, and H. Suzuki, J. Phys. Soc. Jpn. **78**, 084716 (2009).